Lab on a Chip

RSC Publishing

PAPER

Fabry-Pérot cavity sensor-based optofluidic gas chromatography using a microfabricated passive preconcentrator/injector

Cite this: *Lab Chip*, 2013, **13**, 851

Jung Hwan Seo,[ab] Jing Liu,[ad] Xudong Fan[ad] and Katsuo Kurabayashi*[abc]

This study reports on dual on-column Fabry-Pérot (FP) cavity sensor-based gas chromatography (GC) of mixtures of volatile organic compounds (VOCs) utilizing an on-chip device, the so called ''microfabricated passive preconcentrator/injector (μPPI)''. Comprehensive analysis of the sampling, desorption/injection, and compound separation performance of the μPPI-based optofluidic GC system is described. Here, the combined use of the μPPI and on-column FP cavity sensors in a common GC platform enabled diffusion-based passive sampling, rapid (<7 min) chromatographic separation, and optical detection for the quaternary VOC mixtures of benzene, TCE, toluene, and *m*-xylene at sub-ppm concentrations with a simpler fluidic setup than conventional GC systems. The FP cavity sensor arrangement provided the means to study the dynamics of the thermal desorption/injection of VOCs by the μPPI and its effect on the GC separation resolution. Our analysis of obtained chromatograms revealed a presence of the competitive adsorptions of VOC mixtures onto the adsorption sites of trapping materials in the μPPI, which decreased the effective sampling rate by ~50% for compounds with high volatility. The validated performance of the optofluidic GC system promises future development of a field deployable GC microsystem incorporating the μPPI and the FP cavity sensors.

Received 4th October 2012,
Accepted 10th December 2012

DOI: 10.1039/c2lc41119a

www.rsc.org/loc

Introduction

Microscale gas chromatography (μGC) represents the most promising technology for complex volatile organic compound (VOC) mixture analyses in real-time air monitoring, point-of-care biomedical diagnostics, homeland security, and worker exposure assessment. Most μGC systems consist of fluidically interconnected subsystems: a preconcentrator/injector, a separation column, a detector, and a pump.[1–5] These subsystems are typically microfabricated using silicon micro-electromechanical system (MEMS) technology.[6–23] Miniaturization enabled by microfabrication allows rapid temperature programming of the GC subsystems with low power, which is critical for the development of a battery-operated handheld GC system. In particular, a microfabricated preconcentrator (μ-preconcentrator) is one of the key components of a μGC system due to its ability to enhance the system's detection sensitivity by trapping and accumulating low-concentration VOCs. Due to the limited sensitivity of existing gas sensors,[24–26] a μGC system without a μ-preconcentrator is rarely able to detect VOCs at the parts-per-billion (ppb) concentration level, which is required in many applications. A μ-preconcentrator additionally serves as a vapor injector, delivering plugs of the preconcentrated VOCs to a downstream separation column by thermal desorption. The injection sharpness critically affects the separation resolution of a GC system.[27] Therefore, the device must be capable of generating sharp injection plugs. Microfabricated preconcentrator devices developed in previous studies[8–14] generally require substantial energy for both carrier gas pumping and VOC thermal injection.

In our previous work, we demonstrated diffusion-based passive sampling of low-concentration toluene using our on-chip device, namely the ''microfabricated passive vapor preconcentrator/injector (μPPI)'' (Fig. 1A).[28] The μPPI first achieved a sampling rate of 9.1 mL min^{-1} for toluene in an air sample. Subsequently, temperature ramping of an integrated micro-heater allowed the μPPI to release and inject the collected vapor sample at a low heating power of ~1 W and a carrier gas flow rate of 50 mL min^{-1} with an injection sample loss of <5%. The μPPI device is the *first* microfabricated GC component that has the potential to realize zero-power on-chip VOC sampling and low-power injection because of its low power consumption. In addition, our other previous work[29,30]

[a]*Engineering Research Center for Wireless Integrated Microsensing and Systems (WIMS2), University of Michigan, Ann Arbor, MI 48109, USA*
[b]*Department of Mechanical Engineering, University of Michigan, Ann Arbor, MI 48109, USA. E-mail: katsuo@umich.edu; Fax: +1-734-647-3170; Tel: +1-734-615-5211*
[c]*Department of Electrical Engineering and Computer Science, University of Michigan, Ann Arbor, MI 48109, USA*
[d]*Department of Biomedical Engineering, University of Michigan, Ann Arbor, MI 48109, USA*

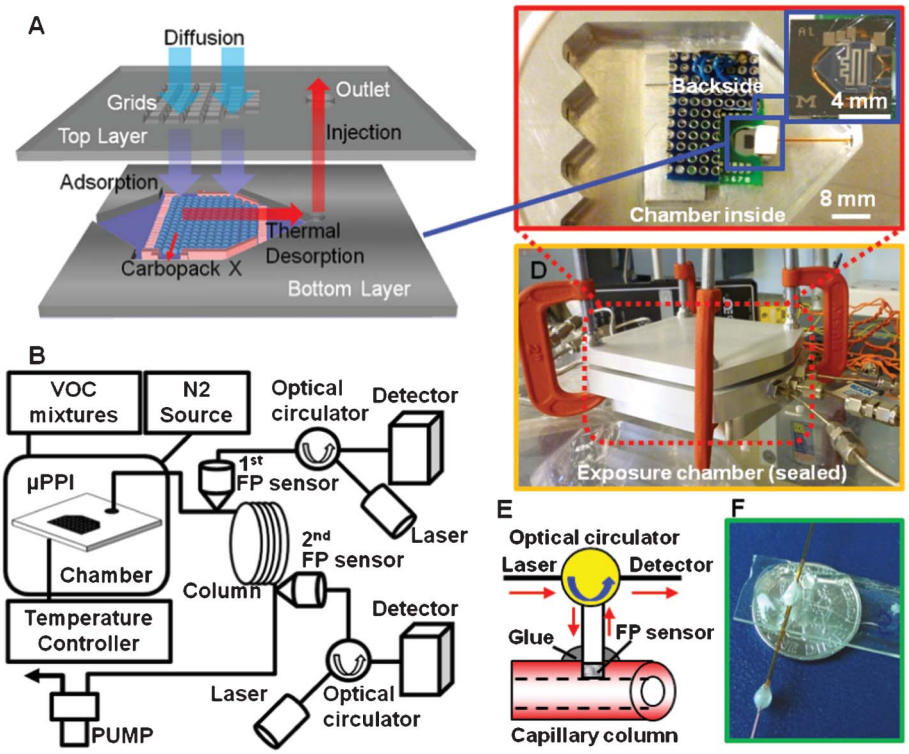

Fig. 1 (A) Conceptual diagram of the μPPI showing the sampling of VOC mixtures by diffusion and thermal desorption/injection processes. The μPPI has a two-layer structure; the top layer incorporates vertical square diffusion channel grids for passive vapor sampling; and the bottom layer contains a membrane cavity structure with tapered entrance/exit on its two sides, pillar structures to retain the graphitized carbon granules inside, and an integrated heater and a resistance temperature detector (RTD) on its backside. (B) Schematic of the optofluidic GC setup incorporating the μPPI and two Fabry-Pérot (FP) cavity interferometric gas sensors. The system enables passive sampling, desorption/injection, and separation of VOC mixtures with a significantly simplified fluidic pathway. (C) Optical image of the μPPI mounted in the exposure chamber. Inset images show the micro-heater and RTD sensor on the backside of the μPPI. (D) Optical image of the sealed exposure chamber. (E) Conceptual diagram of the on-column FP sensor showing its working principles. (F) Optical image of the FP cavity gas sensor assembly.

independently developed a novel on-column GC optical sensor module. The sensor module consisted of a Fabry-Pérot (FP) cavity formed by a two-layer stack of light reflecting/transmitting thin metal coating and gas-sensitive polymer film, which was deposited on the tip of an optical fiber inserted into a separation column. This FP cavity sensor module enabled the acquisition of chromatograms at any arbitrary point along a GC column and was easily adaptable to multipoint on-column detection while integrated with other μGC components, such as microfabricated pumps and columns.[7] Integrated together, the μPPI and the FP cavity sensor module expect to ultimately serve as sub-components of a μGC system with improved separation capability and selectivity, such as a tandem-column system with each column being coated with a different polymer.[21,32–38]

In this article, we explore a complete GC operation that entails sampling, desorption/injection, separation, and detection of VOC mixtures with a broad spectrum of analytes using our μPPI and the on-column FP sensors. Through this demonstration of the GC operation, we aim to show the feasibility of system integration of these two emerging devices in a common GC instrument platform. Hence, we have developed a custom optofluidic GC system employing the μPPI in front of a separation column and two on-column FP sensors at both ends of the separation column (Fig. 1B). Conventional vapor sensors, such as a flame ionized detector (FID) and a photo ionization detector (PID), break down VOC sample molecules and ionize them during the vapor detection process. This sensor operation makes impossible recovery of the original VOC sample for any other subsequent measurements. As a result, a FID or a PID is only installed as the end-point component of a GC instrument. In contrast, the FP sensors in our optofluidic GC system are able to detect *in situ* the vapor signals at both of the column inlet and outlet. This sensor arrangement uniquely provides the means to directly observe vapor mixture injection profiles of the μPPI as well as accurately measure the retention time for each analyte to pass through the separation column.

Using the optofluidic GC system, we verify that the μPPI can (1) sufficiently collect a quaternary mixture containing highly common VOC species as well as single individual analytes on the basis of a zero-power diffusion process and (2) generate a sharp pulse of these concentrated vapors by thermal desorption to obtain sufficiently high separation resolution. To perform quantitative measurements with the FP sensors, we first calibrate the sensor signals at the column outlet for each of the 4 vapor analytes, each having different diffusivity, volatility, and affinity. We next determine the sampling rates

of the μPPI for these analytes. Then, an optimal heating condition of the μPPI is explored to generate a sharp vapor injection profile leading to complete separation of the quaternary VOC mixture while preventing a device failure due to thermal shock. Finally, chromatograms obtained by the complete separation are analyzed and quantified. This allows us to quantitatively characterize the detection sensitivity enhancement for each analyte species and the μPPI's vapor sampling performance in the presence of competing adsorptions of the different VOC components in the quaternary mixture sample. The μPPI-enabled passive VOC sample trapping eliminates the need for a set of multiple pump operations and valve actuations, which is solely responsible for complicated fluidic pathways typically found with conventional GC instruments.[1–5] As such, our optofluidic GC system based on the passive sampling process permits quantitative differentiation and identification of the components of a quaternary VOC mixture with a much simpler fluidic setup than conventional GC instruments.

Materials and methods

Materials

Our experiment used 4 different individual VOCs (benzene, TCE, toluene, and *m*-xylene) that represent a broad spectrum of VOCs ranging from low- to high-volatility compounds (8.29–95.2 torr).[31] The detailed properties of these compounds are given in Table 1. All VOC analytes with purity >99% were purchased from Sigma-Aldrich (St. Louis, MO) and were used as received. A non-polar dimethylpolysiloxane (PDMS) coated separation column (HP-1, i.d. = 250 μm) was obtained from Agilent Technologies Inc. (Santa Clara, CA). For the GC separation tests, we prepared test atmospheres of VOC mixture comprising the 4 different analyte compounds (*i.e.*, benzene, TCE, toluene, and *m*-xylene) in the N_2 gas of a Tedlar bag of 10 L. The concentration of each component in this VOC mixture sample was 50 ppb. Carbopack Xs (C-X, specific area = 250 m^2 g^{-1}, 60/80 mesh) graphitized carbon beads, which were used as the adsorbent materials of the μPPI, were purchased from Supelco (Belafonte, PA) and were used as the adsorbents packed (~750 μg) in the μPPI. The separation column and C-Xs were preheated for cleaning at 250 °C before use.

Experimental setup

To demonstrate the concurrent operation of the μPPI and the FP cavity sensors for GC analysis of VOC mixtures, we built a custom optofluidic GC system based on the chamber test setup (Fig. 1C and 1D). As shown in Fig. 1B, the μPPI-mounted exposure chamber system was fluidically interconnected to two on-column FP cavity sensors,[29,30] a separation column, and a mini-pump. The VOC sample in the N_2 carrier gas was drawn into the system by a mini-diaphragm pump (BTC IIS, Parker, Cleveland, OH). The FP cavity sensors were installed at the both ends of a 10 m long (250 μm (i.d.)) stationary phase coated tubular separation column (HP-1, Agilent, Santa Clara, CA). The incident light coming from the external laser source was coupled into the sensor through an optical circulator and then partially reflected on the metal layer and the interface of the polydimethylsiloxane (PDMS) layer and air, generating an interference spectrum. When the PDMS layer of the sensor was exposed to VOC analytes, the surface interaction between the polymer and the analytes caused a shift of the interference spectrum. This spectrum shift provides the real-time kinetic information for the VOC analytes.

Table 1 List of quaternary compounds and their vapor pressures (p_v), diffusion coefficients (D_0), and molecular weights (MW)

	Properties		
VOC analyte	p_v (torr)	D_0 (cm^2 s^{-1})	MW (g mol^{-1})
Benzene	95.2	0.0932	78.11
TCE	69	0.0875	131.39
Toluene	28.4	0.0849	92.14
m-Xylene	8.29	0.0670	106.16

Microfabrication of the μPPI and the on-column sensor

Detailed information on the processing steps of the μPPI device was provided in our previous study.[28] The fabrication and assembly of the on-column FP sensor were also previously reported.[29] Briefly, the μPPI was fabricated using bulk micromachining based on the growth of a thin thermal oxide layer, Si deep reactive ion etch (DRIE), SiON dielectric thin-film deposition, integrated metallic heater/temperature sensor patterning, selective ethlenediamine pyrocatechol (EDP) wet etch of boron-doped silicon, and modified eutectic wafer bonding. The sensor was fabricated by sequential deposition of a metal layer, such as gold or silver, and a PDMS layer on the end-face of a single mode optical fiber to create a FP cavity (Fig. 1E and 1F).

Sensor signal calibration

The sensing signals rely on sorption characteristics between the PDMS layer of the optical sensor and VOC analytes. To quantitatively assess the performance of our custom GC setup, we calibrated the signals of the on-column FP cavity sensor at the column end for the 4 individual VOCs. We first removed the μPPI-mounted exposure chamber, the first FP cavity sensor at the column inlet, and the column from the test setup, and then connected a Tedlar bag containing benzene vapor of 3 ppm to the setup. The benzene sample in the Tedlar bag was then injected into the second on-column FP cavity sensor, installed at the outlet of the separation column, for 10 s at a flow rate of ~2.0 mL min^{-1} generated by the mini-pump. The peak signal of the injected vapor was monitored in real-time and was recorded at a rate of 20 Hz, using a customized LabView program. The same tests were consecutively performed for the additional 4 different concentrations of 4 ppm, 5 ppm, 6 ppm, and 10 ppm in order to obtain a calibration curve showing the correlation of the peak area and the concentration of analyte (benzene) in the tested sample volume. The vapor mass was calculated from the concentration and the sample volume used (sample injection time × flow rate). We then repeated these tests for other analytes of TCE, toluene, and *m*-xylene.

Sampling rate measurement for 4 individual VOCs with the μPPI device To quantify the μPPI's passive vapor sampling capability upon exposure to various VOCs, we steadily passed *each* of the 4 different analytes (benzene, TCE, toluene, and *m*-xylene) through the exposure chamber containing the device for discrete periods of 15, 30, 45, 60, or 90 min while maintaining each analyte concentration at 500 ppb. In this particular test, we removed the separation column and the first on-column FP cavity sensor, installed at the inlet of the separation column, from the setup and only used the second on-column FP cavity sensor for detection. After each sampling was completed, we covered the diffusion channels of the μPPI top layer with a glass, and next purged the chamber for 1 min with nitrogen gas at $\sim$1 L min^{-1} to remove any residual VOC analyte. The N_2 flow through the chamber was then stopped and we rapidly heated the μPPI from room temperature to $\sim$300 °C for 30 s to desorb the trapped vapors. The released vapors were drawn through the device outlet port to the sensor at a flow rate of 10 mL min^{-1} by the mini-pump, and the mass of each vapor injected by the μPPI was measured using the on-column FP cavity sensor.

Separation and sampling rate measurement of VOC components in the mixture

A VOC mixture sample was passed through the exposure chamber for discrete periods of 15, 30, 45, 60, or 90 min by the mini-pump and was collected by the μPPI. The analytes in the mixture sample were passively trapped within the μPPI in the presence of competing adsorptions on the C-Xs during the sampling process. We next temporally covered the top layer of the device with a glass chip to avoid sample loss from the diffusion channels during the thermal desorption. The device was then heated up to $\sim$300 °C at varying heating rates of the integrated Ti/Pt meander-line micro-heater. The thermally desorbed analytes were delivered to the first on-column FP optical sensor at a flow rate of $\sim$2 mL min^{-1}, which is typically used in GC analysis, during the thermal desorption from the μPPI. The first sensor was used to measure the delivery time of superimposed injection band peaks of the four VOCs thermally desorbed from the μPPI to the column inlet (Step 1 in Fig. 2). These vapors were then drawn into the separation column which was maintained at $\sim$80 °C, and were separated due to the different analyte volatilities (Step 2 in Fig. 2). We next obtained complementary chromatograms for the VOC mixture using the second on-column FP optical sensor (Step 3 in Fig. 2). Finally, we analyzed and quantified the obtained chromatogram peaks for each sampling time, thereby characterizing the effective sampling rate for each analyte species.

Results and discussion

Calibration of the on-column FP cavity sensor

Our results show unique responses of the on-column FP cavity gas sensor to the 4 different analyte compounds. Calibration tests were run in triplicate for each analyte. The relative standard deviation was <10% in all cases. A calibration curve for each analyte was provided by the correlation between the

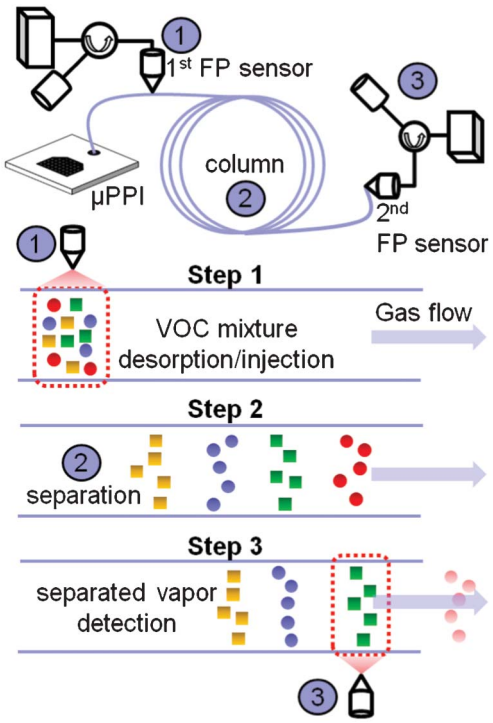

Fig. 2 Working principle of the optofluidic GC technique employing the μPPI and dual on-column FP cavity gas sensors. Thermally desorbed VOC mixtures by the μPPI are detected at the first FP sensor (Step 1). Quaternary analytes separated in the separation column (Step 2) are sequentially observed at the second FP sensor (Step 3).

area of the sensor signal peak and the analyte concentration in the tested sample volume, which enabled the quantitative measurement of vapor mass from the chromatograms. Fig. 3 shows a set of calibration curves for 4 individual vapors of benzene, TCE, toluene, and *m*-xylene obtained by collecting samples for 10 s at a flow rate of $\sim$2 mL min^{-1} for 5 different concentrations of 3, 4, 5, 6, or 10 ppm. The sampled masses achieved from 3 ppm (1.0 ppm mL) to 10 ppm (3.3 ppm mL) range from 3.5 ng to 11.7 ng for benzene, 5.8 ng to 19.4 ng for TCE, 3.7 ng to 12.2 ng for toluene, and 4.6 ng to 15.3 ng for *m*-xylene. As shown in Fig. 3, peak responses increased linearly with the concentration ($r^2 > 0.99$). At a given concentration of 6 ppm (2.0 ppm mL), the corresponding peak areas were 0.202 (benzene), 0.296 (TCE), 0.399 (toluene), and 0.717 (*m*-xylene).

Sampling rate tests for individual VOCs

Fig. 4 shows plots of individually sampled mass *versus* sampling time from 15 to 90 min for each of benzene, TCE, toluene, and *m*-xylene. For each data point, sampling rate tests were run in triplicate and the standard deviation was less than 10%. All the sampled mass in the μPPI was delivered to the optical sensor with no residual analyte in the chamber headspace. This was because we covered the diffusional grids of the top layer of the device with a glass chip. This prevented vapor loss escaping through the diffusion channels by back-diffusion during the desorption process. The results indicate that the sampling performance of the μPPI was consistent and

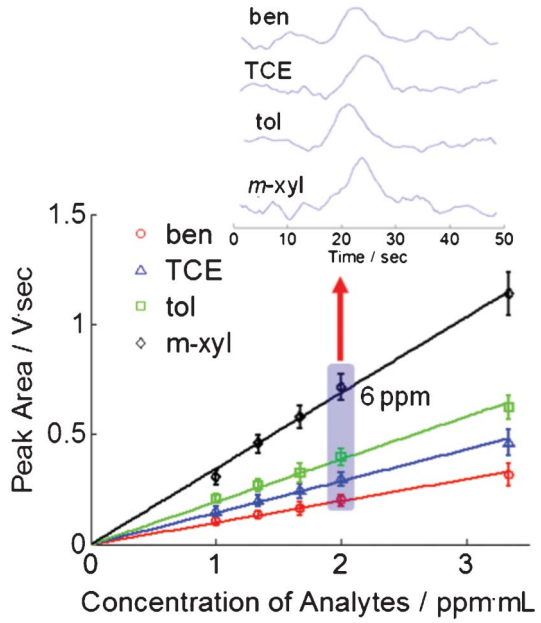

Fig. 3 Calibration curves generated from injecting different concentrations of 4 individual analytes in Tedlar bags to the on-column FP cavity sensor. Samples were injected to the sensor for 10 s at 2 mL min^{-1}. The tested concentrations (corresponding total masses (ppm mL)) ranged from 3 ppm (1.0 ppm mL) to 10 ppm (3.3 ppm mL). THe linear regression r^2 values for all analytes are all >0.99. The inset shows chromatograms of 4 individual analytes (benzene, TCE, toluene, and *m*-xylene) at the concentration of 6 ppm (2 ppm mL).

reproducible for each analyte over the entire series of experiments.

For all the VOC analytes tested in the experiments, Fig. 4 indicates that the mass uptake rates were constant up to ~45 min ($r^2 > 0.99$) at a given concentration of 500 ppb. Sampling rates of 8.7 mL min^{-1}, 8.6 mL min^{-1}, 9.0 mL min^{-1}, and 6.9 mL min^{-1} were obtained from the slopes of the linear region of the curves for benzene, TCE, toluene, and *m*-xylene, respectively. Using the sampling rate equation in our previous study[28] and the diffusion coefficients of these analytes in Table 1, we obtained the theoretical prediction values of 10.2 mL min^{-1} (benzene), 9.6 mL min^{-1} (TCE), 9.3 mL min^{-1} (toluene), and 7.3 mL min^{-1} (*m*-xylene), respectively. These experimental values were 3% (toluene, 9.0 mL min^{-1}) −15% (benzene, 8.7 mL min^{-1}) lower than the theoretical predictions. The corresponding mass uptake rates for the experimental data were 13.9 ng min^{-1} (benzene), 23.2 ng min^{-1} (TCE), 16.7 ng min^{-1} (toluene), and 15.0 ng min^{-1} (*m*-xylene). The discrepancies between the experimental sampling rate and the theoretical prediction were more significant for benzene (15%) and TCE (10%) than the other analytes (3–5%). By taking the narrow linear region up to 30 min, the discrepancies for benzene and TCE became 9% (9.3 mL min^{-1}) and 7% (8.9 mL min^{-1}) lower than predicted by the sampling rate equation, respectively. Yet the errors for these analytes might be caused by relatively lower dynamic responses to the optical sensor due to their higher volatilities.

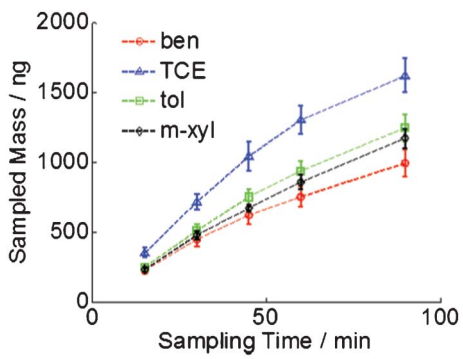

Fig. 4 Plots of the mass trapped and thermally desorbed by the μPPI as a function of sampling time for each analyte at a concentration of 500 ppb. The reduction in the mass uptake rate beyond 45 min for all analytes reflects the decline of the sampling rate as the number of available surface sites on the adsorbents gets decreased.

Beyond ~45 min, the μPPI continued to trap the vapor sample, but at a lower sampling rate for each analyte. This sampling process is expected to continue to decrease until the surface adsorption sites on the adsorbents (C-Xs) get completely filled. At the sampling time of 90 min, the mass uptakes for 4 individual analytes of benzene, TCE, toluene, and *m*-xylene were 0.99 μg, 1.62 μg, 1.25 μg, and 1.17 μg, respectively. As a result of the decline in the sampling rate, these values, sequentially, were 68%, 70%, 80%, and 82% of the total amounts expected (*i.e.*, benzene: 1.47 μg, TCE: 2.33 μg, toluene: 1.55 μg, *m*-xylene: 1.43 μg) assuming the designed constant sampling rate on each of analytes.

Thermal desorption/injection of VOC mixtures by the μPPI

Our previous study[27] indicates that a higher heating rate yields a sharper injection profile with the μPPI. A sharp injection profile is expected to provide high chromatogram resolution. However, our device reliability test indicated that a heating rate of 300 °C s^{-1} resulted in a device failure due to thermal shock. Thus, we monitored *in situ* vapor injection profiles of the μPPI using the first on-column FP cavity sensor installed at the column inlet prior to the separation by gradually increasing the heating rate from 60 °C s^{-1} to a higher value. Here, the injection time (t_i), *i.e.*, the time for the desorbed analytes to travel from the μPPI to the column inlet, was monitored at the heating rates of 60 °C s^{-1}, 75 °C s^{-1}, and 90 °C s^{-1}. (Fig. 5). As expected from the result in our previous study,[27] the superimposed peak signal enhancement of VOC mixtures was reflected in the decrease from 34.3 s to 20.8 s in the full width at half maximum (FWHM) value along with the increase of heating rate from 60 °C s^{-1} to 90 °C s^{-1}. It was also shown that the peak tailings of VOC mixtures were decreased by the increasing heating rate. Based on these superimposed peak signal profiles, we found that the injection time was consistently ~60 s from the instance of time at which the integrated heater of the μPPI was turned on ($t = 0$) regardless of the heating rates. The accurate retention time data obtained by our GC setup promises to facilitate the differentiation and identification of the compounds.

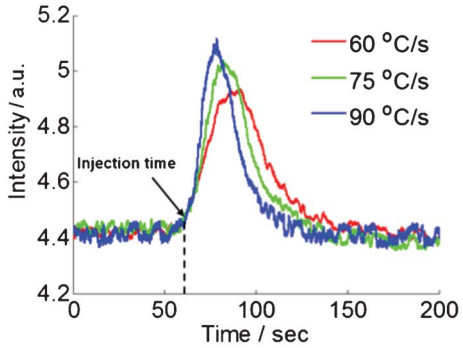

Fig. 5 Experimental plots of the superimposed peak signals of the released VOC mixtures generated by the μPPI at the different heating rates of 60 °C s^{-1} (red), 75 °C s^{-1} (green), and 90 °C s^{-1} (blue). The released/injected peak band signals of VOC analytes are detected at the first FP optical sensor in the custom GC system prior to separation. The reference time point (t = 0) is the time at which the heating power starts to be applied to the μPPI for thermal desorption.

Effect of heating rate on vapor separation performance by the μPPI

Fig. 6 shows the chromatograms corresponding to the injection profiles at the heating rates of 60 °C s^{-1} (0.7 W), 75 °C s^{-1} (0.9 W), and 90 °C s^{-1} (1.1 W). The 4 different analyte VOCs injected into the column were separated in <400 s by means of their different interactions with the stationary phase of the column. The chromatogram data were collected by the second on-column FP optical sensor in the optofluidic GC system. The accurate retention time for each separated analyte was obtained by subtracting t_i from the time (t_0) it took for the peak height signal of each vapor monitored at the column outlet to appear. Benzene and TCE have similar retention time values of ~59 s (t_0: 119 s) and ~90 s (t_0: 150 s), respectively, shorter than the other analytes of toluene (~188 s (t_0: 248 s)) and *m*-xylene (~319 s (t_0: 379 s)). Fig. 6A and 6B indicate that the peak signals of benzene and TCE overlapped each other at both heating rates of 60 °C s^{-1} and 70 °C s^{-1} generated from the μPPI while toluene and *m*-xylene were clearly separated even at the lower heating rate of 60 °C s^{-1}. For the maximum heating rate condition of 90 °C s^{-1}, the eluted peak of benzene was distinctly differentiated from that of TCE (Fig. 6C). The peak height was also significantly enhanced by ~73%, ~37%, ~70%, and ~52% for benzene, TCE, toluene, and *m*-xylene, respectively, compared to that for the lowest heating rate of 60 °C s^{-1}. Here, it would be possible to obtain more enhanced chromatograms at a higher heating rate than 90 °C s^{-1}. However, we used this heating rate for our further analyses as a sufficiently high value to avoid the aforementioned thermal damage to the device.

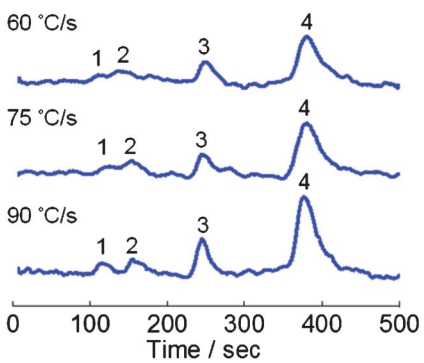

Fig. 6 Chromatograms from the second on-column FP cavity gas sensor for the 3 different heating rates of 60 °C s^{-1}, 75 °C s^{-1}, and 90 °C s^{-1}, generated by the μPPI. Peak assignments are as follows: 1, benzene; 2, trichloroethylene (TCE); 3, toluene; 4, *m*-xylene.

Effective sampling rates of VOC analytes in the mixture

Low volatility compounds are often easily trapped on the adsorption sites of the adsorbents at room temperature, so-called cold trapping, since the analytes have been cooled below their boiling points. The tested mixture sample contained a broad spectrum of VOCs with different vapor pressures, diffusion coefficients, and affinities. Due to these different vapor properties, significant competitive adsorption among these compounds was expected during the sampling process. We used the low concentration of 50 ppb for each component in the mixture sample in order to thoroughly explore how the adsorption sites on the trapping material become occupied with VOC components in the presence of competitive adsorptions for different sampling time periods. Consequent reductions in the sampling rate for each VOC component were quantitatively analyzed by measuring the mass uptake of each analyte from the chromatograms for discrete sampling time periods of 15, 30, 45, 60, or 90 min. The optimal heating rate of 90 °C s^{-1} for thermal desorption/injection was used to provide the sharp injection plugs of the VOC mixture sample to the column, which resulted in the complete separations.

The set of chromatograms in Fig. 7A was generated from the analysis for each of 5 different sampling time periods. As shown, the peak heights of two lower volatile compounds of *m*-xylene and toluene were prominently enhanced along with the increase of the sampling time. This clearly validates the μPPI's analyte preconcentration function leading to high sensitivity required for μGC operations. The mass ratio of the individual analytes in the VOC mixture adsorbed on the surface of the C-Xs was then analyzed as a function of the sampling time (Fig. 7B). Results, plotted in Fig. 7B, show that the mass ratio of *m*-xylene, the lowest volatile analyte among the VOC components, increased at a modest rate up to ~45 min and continued to increase beyond 45 min, but at a lower rate, as the adsorption sites on the C-Xs became occupied. The mass ratio of the second-lowest volatile compound of toluene slightly decreased over time while the ratios of the higher volatile compounds of benzene and TCE decreased at an apparently higher rate. As the sampling time increased from 15 min to 90 min, the masses of benzene, TCE, toluene, and *m*-xylene trapped in the μPPI increased from 19.8 ng to 33.5 ng, from 32.5 ng to 49.1 ng, from 25.4 ng to 63.7 ng, and from 21.8 ng to 140.3 ng, respectively. The relative standard deviation was ⩽15% for benzene and ⩽10% for the rest in all cases. At a sampling time of 90 min, the device trapped the mixture in the mass ratio of 11.7% for benzene, 17.2% for TCE, 22.2% for toluene, and 48.9% for *m*-xylene. Fig. 7C shows plots of sampled mass in the μPPI *versus* sampling time from

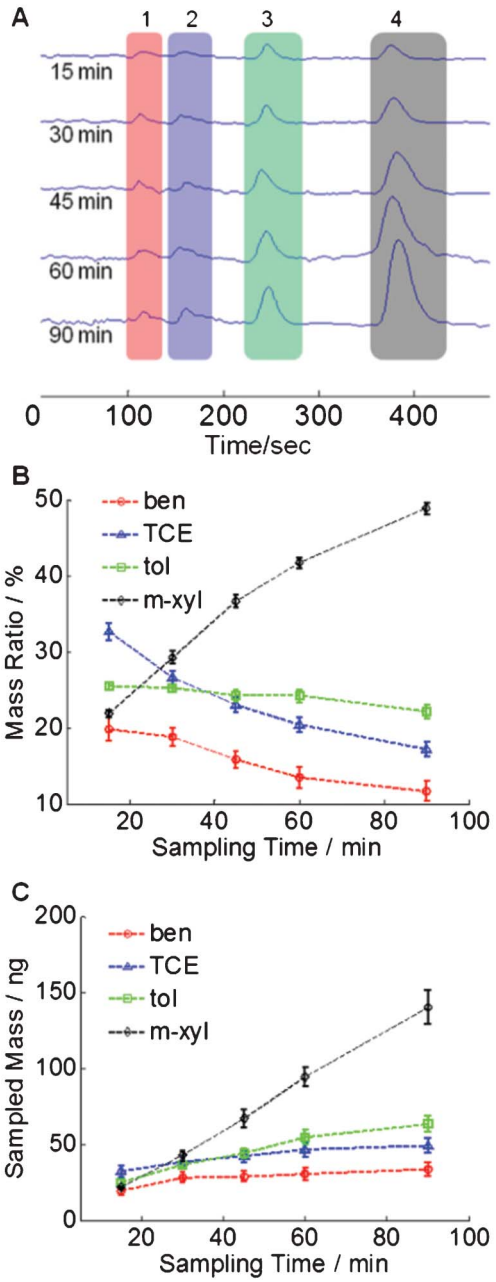

Fig. 7 (A) Chromatograms detected at the second FP cavity sensor for 5 different sampling time periods of 15 min, 30 min, 45 min, 60 min, and 90 min. Peak assignments are as follows: 1, benzene; 2, trichloroethylene (TCE); 3, toluene; 4, *m*-xylene. (B) Plots of mass uptake ratio of the individual compounds of the quaternary VOC mixture adsorbed on the surface of the C-Xs in the μPPI for 5 discrete sampling time periods (15, 30, 45, 60, and 90 min). (C) Plots of sampled mass *versus* sampling time from 15 min to 90 min for each analyte in the VOC mixture sample.

15 to 90 min for each component in the VOC mixture sample. The effective sampling rates of 4.1 mL min^{-1}, 3.5 mL min^{-1}, 5.3 mL min^{-1}, and 6.8 mL min^{-1} were obtained from the slopes of the curves for benzene, TCE, toluene, and *m*-xylene, respectively. These sampling rate values were 52.9% in benzene, 59.3% in TCE, 41.1% in toluene, and 1.5% in *m*-xylene lower than the single analyte exposure test results.

The results, shown in Fig. 7, verify that the competitive adsorptions of VOC mixtures onto the adsorption sites on the C-Xs result in reductions in the effective sampling rate for individual components of the mixture sample. Also, these results indicate that the less volatile vapor is the more preferentially adsorbed on the adsorption sites. Despite the reduction in the effective sampling rate in the presence of the competitive adsorptions among the quaternary mixtures, the μPPI sufficiently trapped all the quaternary mixtures at a low concentration of 50 ppb, thereby enabling the detection peak signal enhancement. To enhance the effective sampling rate for the high volatile compounds, we could use other VOC adsorbent materials with a large surface area (*e.g.*, Carboxen series (500–1500 m^2 g^{-1}), *etc.*), which are typically used to trap highly volatile compounds.

Conclusions

Our fluidically simplified custom GC system incorporating the μPPI and the dual on-column FP cavity sensors was capable of chromatographic analyses of VOC mixture samples. We first characterized the passive preconcentration performance of the μPPI for 4 individual VOC analytes of benzene, TCE, toluene, and *m*-xylene at low concentrations. These analytes represent a broad range of VOCs with different vapor pressures and affinities. The precise chromatographic retention time data obtained for the system facilitated the identification of each component of the VOC mixtures. The calibration data for the optical sensor enabled the quantitative assessment of the chromatographic separation resolution. Our system has the unique ability to observe *in situ* vapor injection profiles upon the thermal desorption process using the μPPI. With this observation, the optimal heating conditions of 90 °C s^{-1} were determined to achieve complete VOC separation with significant elution peak signal enhancement while avoiding thermal shock to the μPPI device. From the chromatogram peak analyses, we determined the competitive adsorptions of the analytes of the quaternary mixture onto the adsorption sites as a function of sampling time. Consequent reductions in the effective sampling rates for the analytes were also explored.

The increase of the sampling time from 15 min to 90 min also resulted in the change of the mass ratio of the quaternary mixture trapped in the μPPI from 19.9% to 11.7% in benzene, from 32.7% to 17.2% in TCE, from 25.5% to 22.2% in toluene, and from 21.9% to 48.9% in *m*-xylene. It follows that the compounds with lower volatility tend to more occupy sorption sites on the adsorbent surface than those with higher volatility in the sampling process. Consequently, we obtained the effective sampling rates of 4.1 mL min^{-1} reduced by 52.9%, 3.5 mL min^{-1} reduced by 59.3%, 5.3 mL min^{-1} reduced by 41.1%, and 6.8 mL min^{-1} reduced by 1.5% for benzene, TCE, toluene, and *m*-xylene, respectively, in comparison to those obtained from the individual analyte exposure tests. Despite the presence of reductions in the sampling rates by these

competitive adsorptions, the separated analytes peak signals were remarkably enhanced even at the short sampling time of 15 min. Thus, sufficient masses of low-concentration VOC analytes could be collected for GC analysis within a few minutes from the environment by virtue of passive diffusion-driven sampling. With the performance of our custom optofluidic GC system verified, the integration of the μPPI and the FP cavity sensors proved to enable low-power, signal-enhanced, high-fidelity GC analyses without requiring a complicated assembly of the conventional fluidic valves and actuators.

Our study indicates that the sampling performance of the μPPI for a particular analyte compound could significantly vary with the analyte composition and compound type of the mixture sample because of the competing adsorption of the analytes with the different relative volatilities, affinities, and diffusivities. For this reason, the analyte profiles detected by our optofluidic GC system are unable to reflect the real composition of complex mixtures and the original masses of the constituent compounds. This issue is primarily attributed to an insufficient amount or adsorptivity of the particular adsorbent material used in the device and/or to insufficient sampling time for highly volatile compounds. To mitigate this issue, our future work will use a sufficient adsorbent mass (or surface area) and sampling time with several different adsorbent materials integrated together in the μPPI. This will enable us to ensure quantitative analysis of the real sample composition. Together with this modification, the technology presented here opens the way for our future development of a field-deployable μGC system incorporating the μPPI and the FP cavity sensors. Ultimately, the μGC system will be tested for personal exposure monitoring to assess the health impacts of VOC analytes.

Acknowledgements

The authors would like to thank Edward T. Zellers for assistance in device design. This work was supported by the Engineering Research Centers Program of the National Science Foundation under Award Number ERC-9986866 and NIOSH Pilot Project Research Training Program (PPRT).

References

1 C.-J. Lu, W. H. Steinecker, W.-C. Tian, M. C. Oborny, J. M. Nichols, M. Agar, J. A. Potkay, H. K. L. Chan, J. Driscoll, R. D. Sacks, K. F. Wise, S. W. Pang and E. T. Zellers, *Lab Chip*, 2005, **5**, 1123–1131.
2 S. Zampolli, I. Elmi, F. Mancarella, P. Betti, E. Dalcanale, G. C. Cardinali and M. Sveri, *Sens. Actuators, B*, 2009, **141**, 322–328.
3 P. R. Lewis, R. P. Manginell, D. R. Adkins, R. J. Kottenstette, D. R. Wheeler, S. S. Sokolowski, D. E. Trudell, J. E. Byrnes, M. Okandan, J. M. Bauer, R. G. manley and G. C. Frye-Mason, *IEEE Sens. J.*, 2006, **6**, 784–795.
4 S. K. Kim, H. Chang and E. T. Zellers, *Anal. Chem.*, 2011, **83**, 7198–7206.
5 J. A. Dziuban, J. Mróz, M. Szczygielska, M. Małachowski, A. Górecka-Drzazga, R. Walczak, W. Buła, D. Zalewski, Ł. Nieradko, J. Łysko, J. Koszur and P. Kowalski, *Sens. Actuators, A*, 2004, **115**, 318–330.
6 H. Kim, W. H. Steinecker, S. M. Reidy, G. R. Lambertus, A. Astle, K. Najafi, E. T. Zellers, L. P. Bernal, P. Washabaugh and K. D. wise, *Technical Digest Transducers' 07*, Lyon, France, 2007, pp. 1505–1508.
7 J. Liu, N. K. Gupta, K. D. Wise, Y. B. Gianchandani and X. Fan, *Lab Chip*, 2011, **11**, 3487–3492.
8 I. Gràcia, P. Ivanov, F. Blanco, N. Sabaté, X. Vilanova, X. Correig, L. Fonseca, E. Figueras, J. Santander and C. Cané, *Sens. Actuators, B*, 2008, **132**, 149–154.
9 W.-C. Tian, H. K. L. Chan, C-J. Lu, S. W. Pang and E. T. Zellers, *J. Microelectromech. Syst.*, 2005, **14**, 498–507.
10 M. Kim and S. Mitra, *J. Chromatogr., A*, 2003, **996**, 1–11.
11 C. Pijolat, M. Camara, J. Courbat, J.-P. Viricelle, D. Briand and N. F. de Rooij, *Sens. Actuators, B*, 2007, **127**, 179–185.
12 J. Yeom, C. R. field, B. Bae, R. I. Masel and M. A. Shannon, *J. Micromech. Microeng.*, 2008, **18**, 125001.
13 R. P. Manginell, D. R. Adkins, M. W. Moorman, R. Hadizadeh, D. Copic, D. A. Porter, J. M. Anderson, V. M. Hietala, J. R. Bryan, D. R. Wheeler, K. B. Pfeifer and A. Rumpf, *J. Microelectromech. Syst.*, 2008, **17**, 1396–1407.
14 B. Alfeeli, D. Cho, M. Ashraf-Khorassani, L. T. Taylor and M. Agah, *Sens. Actuators, B*, 2008, **133**, 24–32.
15 H.-S. Noh, P. J. hesketh and G. C. Frye-Mason, *J. Microelectromech. Syst.*, 2002, **11**, 718–725.
16 G. Lambertus, A. Elstro, K. Sensenig, J. Potkay, M. Agah, S. Scheuering, K. Wise, F. Dorman and R. Sacks, *Anal. Chem.*, 2004, **76**, 2629–2637.
17 M. Agah, J. A. Potkay, G. Lambertus, R. Sacks and K. D. Wise, *J. Microelectromech. Syst.*, 2005, **14**, 1039–1050.
18 A. Bhushan, D. Yemane, D. Trudell, E. B. Overton and J. Goettert, *Microsyst. Technol.*, 2007, **13**, 361–368.
19 S. Reidy, G. Lambertus, J. Reece and R. Sacks, *Anal. Chem.*, 2006, **78**, 2623–2630.
20 A. D. Radadia, R. I. Masel, M. A. Shannon, J. P. Jerrell and K. R. Cadwallader, *Anal. Chem.*, 2008, **80**, 4087–4094.
21 C.-J. Lu, J. Whiting, R. D. Sacks and E. T. Zellers, *Anal. Chem.*, 2003, **75**, 1400–1409.
22 R. Archibald, P. Datskos, G. Devault, V. Lamberti, N. Lavrik, D. Noid, M. Sepaniak and P. Dutta, *Anal. Chim. Acta*, 2007, **584**, 101–105.
23 G. R. lambertus, C. S. Fix, S. M. Reidy, R. A. Miller, D. Wheeler, E. Nazarov and R. Sacks, *Anal. Chem.*, 2005, **77**, 7563–7571.
24 E. Covington, F. I. Bohrer, C. Xu, E. T. Zellers and C. Kurdak, *Lab Chip*, 2010, **10**, 3058–3060.
25 R. P. Manginell, J. M. Bauer, M. W. Moorman, L. J. Sanchez, J. M. Anderson, J. J. Whiting, D. A. Porter, D. Copic and K. E. Achyuthan, *Sensors*, 2011, **11**, 6517–6532.
26 C. Jin, P. Kurzawski, A. Hierlemann and E. T. Zellers, *Anal. Chem.*, 2008, **80**, 227–236.
27 J. H. Seo, J. Liu, X. Fan and K. Kurabayashi, *Anal. Chem.*, 2012, **84**, 6336–6340.
28 J. H. Seo, S. K. Kim, E. T. Zellers and K. Kurabayashi, *Lab Chip*, 2012, **12**, 717–724.

29 J. Liu, Y. Sun and X. Fan, *Opt. Express*, 2009, **17**, 2731–2738.
30 J. Liu, Y. Sun, D. J. Howard, G. Frye-Mason, A. K. Thompson, S.-J. Ja, S.-K. Wang, M. Bai, H. Taub, M. Almasri and X. Fan, *Anal. Chem.*, 2010, **82**, 4370–4375.
31 G. O. Nelson, *Gas Mixtures: Preparation and Control*, CRC Press, Boca Raton, FL, 1992.
32 M. P. Rowe, W. H. Steinecker and E. T. Zellers, *J. Environ. Monit.*, 2007, **8**, 270–279.
33 J. R. Jones and J. H. Purnell, *Anal. Chem.*, 2002, **62**, 2300–2306.
34 D. R. Deans and I. Scott, *Anal. Chem.*, 2002, **45**, 1137–1141.
35 J. H. Purnell and M. H. Wattan, *Anal. Chem.*, 2002, **63**, 1261–1264.
36 T. Veriotti and R. Sacks, *Anal. Chem.*, 2001, **73**, 813–819.
37 M. Libardoni, M. McGuigan, Y. J. Yoo and R. Sacks, *J. Chromatogr., A*, 2005, **1086**, 151–159.
38 R. Sacks, C. Coutant, T. Veriotti and A. Grail, *J. Sep. Sci*, 2000, **23**, 225–234.